High-resolution seismic imaging of shallow karstified carbonate overburden offshore Indonesia

Xiaobo Li, Yonghe Guo, Yi Xie, Barry Hung (CGG); Ilham Panggeleng, M.R Husni Sahidu, Sarah Putri (BP)*

Summary

Heavily faulted and karstified carbonate overburden poses potential geohazards for well drilling in West Papua, offshore Indonesia. Hence, high-resolution seismic images that capture geological details, such as karstified faults and small-scale caves within the carbonate, are highly desirable. In this study, two aspects play a pivotal role. First is the velocity model, which can capture velocity contrasts that are highly spatially varying within the carbonate. Second, considering the shallow nature of the targeted carbonate layer and the sampling limitation of the Ocean-Bottom Cable (OBC) acquisition, is a solution that handles the associated illumination issue. For the former, we demonstrate with Time-Lag Full-Waveform Inversion (TLFWI) that a high-resolution velocity model that conforms to geology can be obtained, which in turn generates significant uplift in the image using primary reflections. For the latter, we propose to use multiple imaging to further enhance the resolution of the structures within the carbonate. The resulting image provides new insight into the understanding of the fault and karst systems for the well drilling plan.

Introduction

Offshore Papua is the largest gas-producing region in Indonesia. However, designing a drilling plan in this area is a challenging task due to the heavily faulted and intensely karstified carbonate overburden layer (Yudhanto and Pasaribu, 2012; Birt et al., 2015; Birt et al., 2020). The karstified features, such as collapsed caves or karstified fault planes, should be avoided for well planning, otherwise, they can lead to hole-cleaning problems, pack-offs, and stuck pipes (Birt et al., 2020). Thus, high-resolution images that can identify these small geological features are highly desirable. A recent study brought better understanding for similar geological settings by revealing complex faults and small-scale caves with very high-density Ocean-Bottom Node (OBN) data. This has made a significant impact on well planning and drilling operations (Wolfarth et al., 2019; Birt et al., 2020). Here， we propose to see if the knowledge and lessons learned from that study are transferable to other areas in this region for better shallow imaging of the carbonate layer.

In this study, we focus on a neighboring survey with OBC data that was acquired in 2010. The receiver line and receiver point intervals were 450 m and 25 m, respectively. The shot line spacing was 150 m with zigzag 25 m shot point spacing. Figure 1 shows an example of a legacy image from south-west to north-east in this area. Figure 1b depicts a zoomed-in section of the shallow carbonate, which was the target area of this study. The carbonate overburden extended from 100 m to 1800 m without much coherent seismic energy due to scattering and attenuation within the carbonate layers. The legacy volume provided clearer imaging of the top of the carbonate towards the north-east direction than towards the south-west direction, where the top of carbonate was close to the seafloor (as indicated by the red and green arrows in Figure 1b). Within the carbonate layer, there were incoherent signals contaminating karstified caves, as highlighted by the blue arrow in Figure 1b. Thus, the resolution of the legacy image was not sufficient to meet the requirements for well planning.

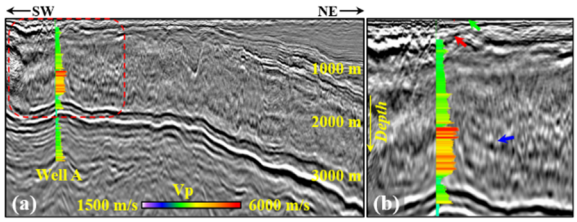

Figure 1: (a) Cross-section from south-west to north-east of legacy Kirchhoff PSDM image overlaid with P-wave velocity log; (b) zoomed-in view of the focus area of the new processing, as highlighted by the red dashed rectangle in (a).

To reveal the complex overburden image, an accurate velocity model is very important. In this shallow water area (10~60 m), the seismic velocity varies rapidly, as illustrated by the sonic log information in Figure 1b. Due to the heavily karstified phenomenon within the carbonate layer, strong heterogeneous local velocity anomalies were observed within the same carbonate sequence (Birt et al., 2020), which may correspond to cave structures, as indicated by the blue arrow in Figure 1b. It is challenging for conventional tomography to derive a high-resolution velocity model within the carbonate layer to identify these structures since it requires coherent reflectors for the inversion. TLFWI (Zhang et al., 2018) has demonstrated that it is an effective tool for inverting a high-resolution velocity model, even for small-scale velocity anomalies (Vandrasi et al., 2020; Salaun et al., 2021; Wei et al., 2021; Zhang et al., 2021).

In addition to a high-resolution velocity model, high-end imaging is another key factor. The seabed in this area is very shallow, as seen in Figure 2b, and the data was acquired on a sparse grid. Hence, primary reflections suffered from poor spatial sampling and could not provide sufficient information for shallow imaging. Moreover, the seismic responses of karstified geological abnormalities were mainly diffractions, which made primary-only imaging more difficult with sparse data. Multiple migration (Poole, 2021)

was thus a good candidate to address this challenge by benefiting from the near-angle illumination of multiples.

To overcome the seismic imaging challenges for the complex carbonate overburden, TLFWI was applied to derive a detailed velocity model, and then both primaries and multiples were used to optimize the shallow images. The new results provided an integrated solution to reveal the heavily faulted and karstified carbonate overburden.

High-resolution model from TLFWI to improve the definition of karstified faults in the primary image

As the top of the carbonate was very shallow in this case, rich diving waves were observed in the recorded data (see the raw shot gather in Figure 2a). Moreover, the complex carbonate layer in this area is known to manifest strong azimuthal effects (Birt et al., 2020). This can be illustrated by Figure 2b, where we can see that the diving waves propagate with obviously differing velocities in different azimuthal directions. In the context of obtaining high-resolution imaging, this gives us a hint that Orthorhombic (ORT) FWI (Xie et al., 2017) is a relevant tool to be considered. With recent successful examples of overcoming cycle-skipping issues with a time-lag cost function (Zhang et al., 2018), ORT-TLFWI was applied for inverting the velocities in this case.

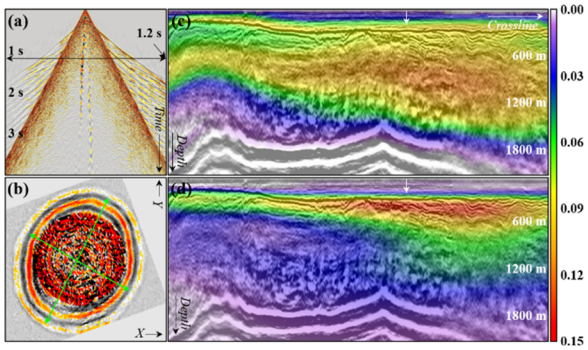

Figure 2: (a) Raw shot gather corresponding to the location indicated by the white arrow in (c) and (d); (b) time slice at 1.2 s of the raw shot gather in (a); (c) inline section of ORT strength (difference of epsilon between fast and slow velocity directions) from 2018 legacy model; and (d) new model after TLFWI. The inline section is just under an individual receiver line and both models are ovelaid on an RTM image obtained with the new model.

Figure 2d displays the epsilon difference between fast and slow velocity directions that was updated by ORT-TLFWI. Comparing with the epsilon field that was obtained by reflection tomography in the legacy result (Figure 2c), we observed that the anisotropic field was not only more geologically conformal in the new result but the epsilon field also had higher resolution. With the help of a better anisotropic field and new algorithm from TLFWI, the resolution of the new velocity was improved significantly. Figures 3b and 3d show a crossline section and the depth slice at 1300 m of the new velocity obtained by 12 Hz ORT-TLFWI. Comparing with the corresponding displays from the legacy velocity (Figures 3a and 3c), the vertical karstified faults were clearly captured in the new model (black arrows in Figure 3b). Localized velocity features within the carbonate and near the top of the carbonate were also well captured (white arrows in Figure 3b). In addition, as observed from the depth slice, heavily karstified fault planes were more well organized in the new model (Figure 3d), and localized velocity features with much higher resolution were identified.

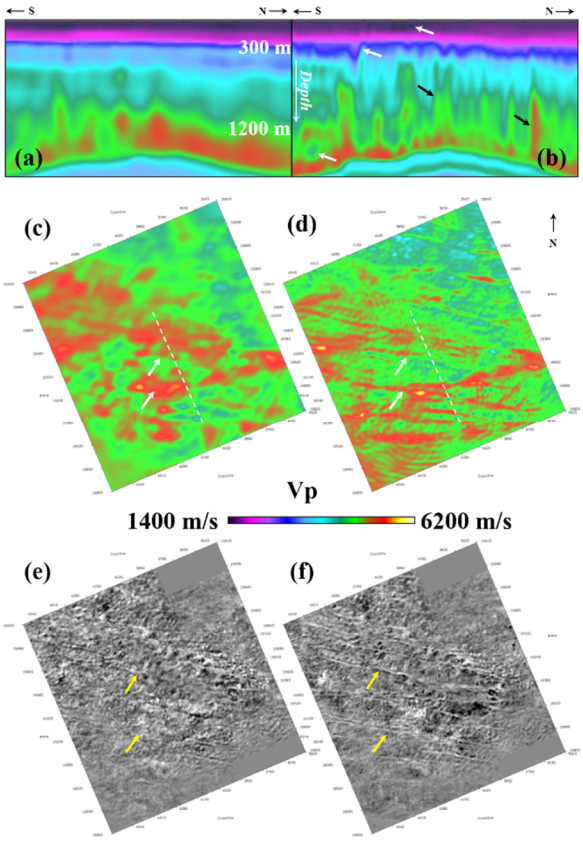

Figure 3: Crossline sections of (a) legacy velocity model, and (b) new velocity model, with the location indicated by white dashed lines in the depth slices at 1300 m of (c) legacy velocity model, and (d) new velocity model. Coreesponding RTM depth slices (e) using legacy model and (f) using new model. The migration input is the final up-going data from the new processing for both (e) and (f).

Reverse Time Migration (RTM) was used to image the primary reflections as it can naturally handle strong spatial

velocity variations. The primary images with the new model (Figure 3f) better reveal the complex fault system and cave features in comparison with the legacy results (Figure 3e). Figure 4 shows a velocity model comparison from a shallower section at 300 m in depth. It is obvious that the new TLFWI model (Figure 4b) provided much higher resolution, while the legacy velocity was very smooth (Figure 4a). However, the primary image (Figure 4c) still suffered from strong footprints at this depth due to the relatively sparse OBC acquisition.

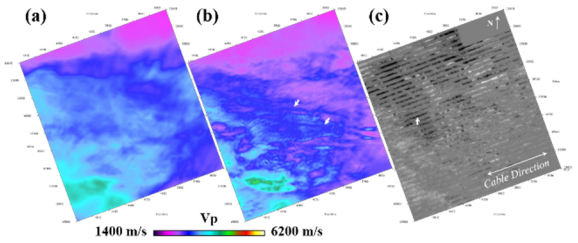

Figure 4: Depth slice at 300 m of (a) legacy velocity model, (b) new velocity model, (c) primary image using new velocity model.

Multiple imaging to reveal the shallow soft channels, collapsed features and karstified caves

As can be observed from the image in Figure 4c, imaging using primary reflections results in the shallow part of the image suffering from illumination issues due to the coarse sampling in the acquisition. Imaging using multiples has been shown to be one way to overcome this issue (Poole, 2021), as multiples contain richer near-angle illumination information than primaries in shallow sections. Multiple imaging of OBC data operates in the common receiver domain, imaging the densely sampled source-side multiples, and thus can provide better high-resolution shallow images thanks to much richer near-angle illumination and extended illumination range contributed by the multiples.

Figure 5 shows a comparison of a shallow depth slice (50 m) and crossline section between primary-only and multiple images. The multiple imaging result (Figure 5c) clearly reveals the shallow channels, while the primary-only image leaves regular holes (Figure 5a). In the crossline (indicated by the green dashed line in the depth slice), the top of the carbonate was broken in the primary image, and strong aliasing noise is evident (Figure 5b) because of the coarse spatial sampling. In contrast, multiple imaging produced much higher resolution images in the very shallow part (Figure 5d). The event continuity around the top of the carbonate was improved significantly, and the aliasing noise in the crossline section was greatly reduced. As a result, the karstified bodies inside the carbonate layer became much clearer in the multiple migration images. (Figure 5d).

Figure 6 shows a comparison between primary imaging and multiple imaging around the top of carbonate. The green line shows the proposed well location. Collapse features were clearly revealed by multiple imaging, as highlighted by the

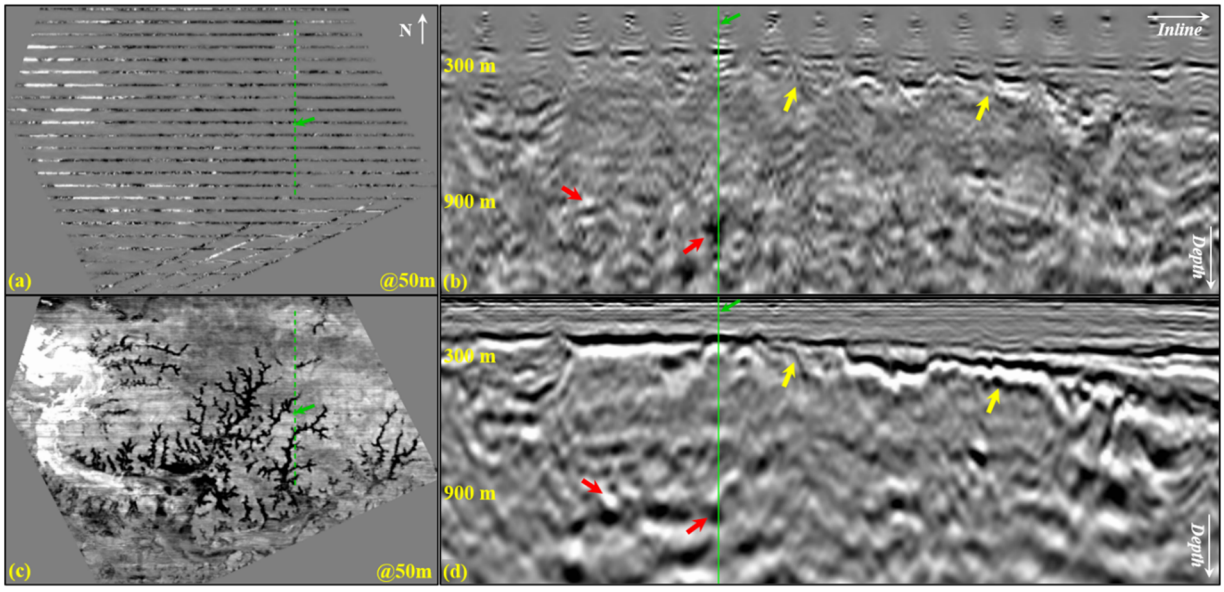

Figure 5: Comparison of Primary Image and Multiple Image: Depth slice at 50 m of (a) Primary Image and (c) Multiple Image, and crossline section of (b) Primary Image and (d) Multiple Image. The green dashed lines on the depth slices show the location of the crossline section. The green solid lines in the crossline sections show the location of a planned well, which corresponds to the location highlighted by the green arrow in the depth slices.

yellow circle in Figure 6b, which were consistent with the hints in the primary images (Figure 6a). The inline section comparison inside the carbonate layer is shown in Figure 7. Thanks to the richer near-angle information from multiples than primaries, the karstified caves along the planned well were more focused and clearer in the multiple images (Figure 7b) than the primary-only images (Figure 7a).

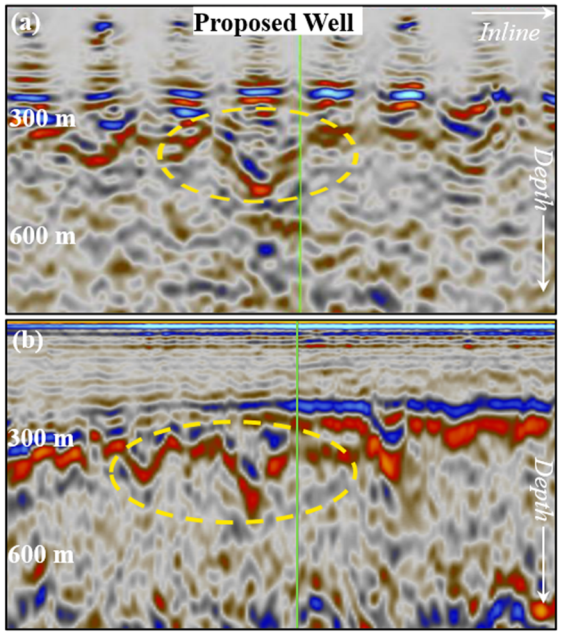

Figure 6: Crossline section around the top of the carbonate layer passing through one proposed well: (a) Primary Image; (b) Multiple Image.

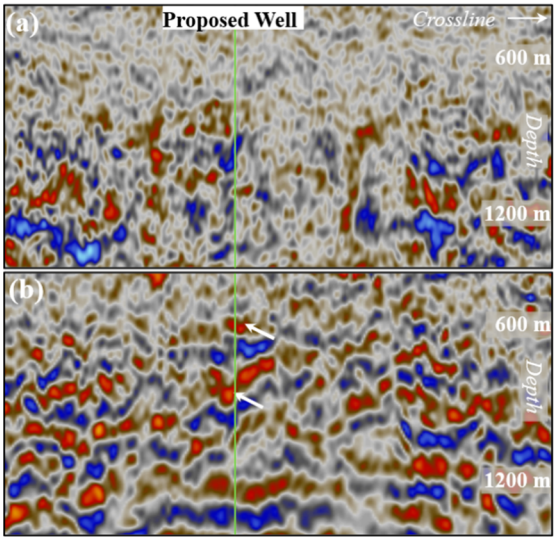

Figure 7: Inline section passing through one proposed well: (a) Primary Image; (b) Multiple Image.

Discussion

This study resulted in improved resolution of the carbonate imaging to reveal detailed faults and caves that allows better correlation with well events (Figure 8). The first occurrence of loss circulation in the shallow section might be related to enhanced karstification at the top of the carbonate due to sub-aerial exposure during the Oligocene tectonics. The next series of losses events down to the bottom of the carbonate layer coincides with brighter amplitudes (white arrows) related to the karst features. The new result provides a more confident interpretation to support well planning activity.

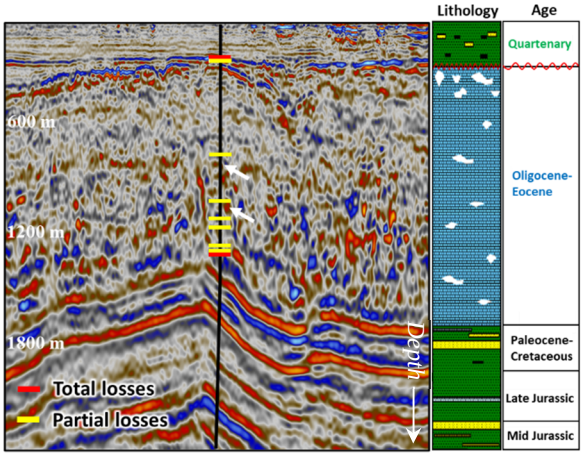

Figure 8: Losses events correlated with karst features observed from the seismic image in this study. Black line indicates the existed well.

Conclusions

Seismic imaging for complex carbonate overburden is very challenging but highly desirable for development drilling offshore Papua. In this study, TLFWI successfully derived a detailed geological model, and the subsequent primary imaging produced significant uplift in defining karstified faults. Multiple imaging further revealed soft channels, collapsed bodies, and karstified caves. The high-resolution channel images with fine branches, which often associated with the presence of shallow gas, are very important to the shallow geohazards assessment in determining the risk-free area for proposed jack-up rig and platform locations. The clear features of collapsed bodies, karstified fault planes, and caves can be used to guide the drilling plan. By fully utilizing all types of the wavefield, the new results provide an integrated solution for complex overburden imaging to help avoiding potential drilling hazards in this region.

Acknowledgments

We thank SKK Migas, BP, and CGG for permission to publish this work. We are grateful to our team for processing the data and Xu Qing and Yu Ziqin for valuable discussions.

REFERENCES

Birt, C., B. Boyd, and A. Nugraha, 2015, Evolution and karstification of the Eocene-Miocene carbonates overlying the Tangguh gas fields in Western Papua—Observations from 3D seismic and impact on drilling operations: Presented at the Proceedings of Indonesian Petroleum Association 39th Annual Convention, IPA15-G-302.

Birt, C., D. Priyambodo, S. Wolfarth, J. Stone, and T. Manning, 2020, The value of high-density blended OBN seismic for drilling and reservoir description at the Tangguh gas fields, Eastern Indonesia: The Leading Edge, **39**, 574–582, doi: https://doi.org/10.1190/tle39080574.1.

Poole, G., 2021, Least-squares multiple imaging constrained jointly by OBN and towed streamer data: 82nd Annual International Conference and Exhibition, EAGE, Extended Abstracts, doi: https://doi.org/10.3997/2214-4609.202113070.

Salaun, N., M. Reinier, I. Espin, and G. Gigou, 2021, FWI velocity and imaging: A case study in the Johan Castberg area: 82nd Annual International Conference & Exhibition, EAGE, Extended Abstracts, doi: https://doi.org/10.3997/2214-4609.202112763.

Vandrasi, V., M. Al-Waily, S. Mothi, and A. Vasquez, 2020, Time-lag FWI based velocity model and image of a coarse shallow water OBC data set: 90th Annual International Meeting, SEG, Expanded Abstracts, 715–719, doi: https://doi.org/10.1190/segam2020-3427971.1.

Wei, Z., J. Mei, Z. Wu, Z. Zhang, R. Huang, and P. Wang, 2021, FWI imaging: Revealing the unprecedented resolution of seismic data: First International Meeting for Applied Geoscience & Energy, SEG/AAPG, Expanded Abstracts, 682–686, doi: https://doi.org/10.1190/segam2021-3583772.1.

Wolfarth, S., D. Priyambodo, P. Deng, X. Li, S. Cao, F. C. Loh, and B. Hung, 2019, Targeted High-End Processing to Deliver a Rapid P-Image from the Tangguh ISS® OBN survey: 81st Annual International Conference and Exhibition, EAGE, Extended Abstracts, We R04 07, doi: https://doi.org/10.3997/2214-4609.201901184.

Xie, Y., B. Zhou, J. Zhou, J. Hu, L. Xu, X. Wu, N. Lin, F. C. Loh, L. Liu, and Z. Wang, 2017, Orthorhombic full- waveform inversion for imaging the Luda field using wide-azimuth ocean-bottom-cable data: The Leading Edge, **36**, 75–80, doi: https://doi.org/10.1190/tle36010075.1.

Yudhanto, E. V., and D. Pasaribu, 2012, Structural evolution of Ubadari Field, Bird's Head, Papua, Indonesia: Presented at the AAPG International Conference and Exhibition, Singapore, September 16–19.

Zhang, J., Z. Wang, Y. Chen, Y. Guo, Z. K. Fong, J. Li, and Y. Wu, 2021, The first high-end OBC imaging for fractured basement in Bohai Bay, China: First International Meeting for Applied Geoscience & Energy, SEG/AAPG, Expanded Abstracts, 2544–2548, doi: https://doi.org/10.1190/segam2021-3587037.1.

Zhang, Z., J. Mei, F. Lin, R. Huang, and P. Wang, 2018, Correcting for salt misinterpretation with full-waveform inversion: 88th Annual International Meeting, SEG, Expanded Abstracts, 1143–1147, doi: https://doi.org/10.1190/segam2018-2997711.1.